Broad luminescence from donor-complexed Li_{Zn} and Na_{Zn} acceptors in ZnO

Y. K. Frodason,[*] K. M. Johansen, A. Galeckas ⬤, and L. Vines

Department of Physics/Centre for Materials Science and Nanotechnology, University of Oslo, N-0318 Oslo, Norway

Zn substitutional lithium (Li_{Zn}) and sodium (Na_{Zn}) acceptors and their complexes with common donor impurities (Al_{Zn}, H_i, and H_O) in ZnO have been studied using hybrid functional calculations. The results show that the complexes are not exclusively charge neutral, but rather exhibit a thermodynamic $(+/0)$ transition level close to the valence band maximum. The positive charge states are associated with a polaronic defect state, similar to those of the well-studied charge-neutral isolated acceptors. This incomplete passivation has profound consequences for the optical properties of the complexes. Indeed, electron transitions from the conduction band minimum to the $(+/0)$ transition level of the complexes result in broad luminescence bands that are blueshifted with respect to those originating from the isolated acceptors. Such complexes are proposed as a potential defect origin of the green luminescence observed at the high-energy side of the orange luminescence band (caused by Li_{Zn}) in hydrothermally grown ZnO. This prediction is supported by experimental photoluminescence and secondary ion mass spectrometry data on a hydrothermally grown ZnO sample. We have also explored how the parameters controlling the fraction and screening of exchange in the Heyd-Scuseria-Ernzerhof (HSE) hybrid functional influence the results by comparing two parametrization approaches: (i) the conventional one where the exchange fraction is adjusted to reproduce the experimental band gap, and (ii) tuning both parameters in order to also comply with the generalized Koopmans theorem (gKT). Interestingly, these approaches were found to yield similar results.

I. INTRODUCTION

The behavior of Li in ZnO has long been the subject of considerable scientific interest. Early experimental work on Li in ZnO by Lander [1] indicated an electrically amphoteric behavior. Subsequent investigations have confirmed that Li can act as an interstitial donor (Li_i) or a Zn substitutional acceptor (Li_{Zn}) [2–8]. Many initial attempts to achieve *p*-type conductivity in ZnO involved the Li_{Zn} acceptor as a potential shallow dopant, with the amphoteric behavior of Li and consequent Fermi level pinning as the main hindrance. However, it is now widely agreed that Li_{Zn} introduces a deep acceptor level [9,10]. Indeed, the paramagnetic Li_{Zn}^0 state can be observed by electron paramagnetic resonance (EPR) spectroscopy, and corresponds to a small hole polaron localized at one of the four O^{2-} ions immediately adjacent to Li_{Zn} [2,11,12].

The optical properties of Li in ZnO have also been studied extensively. EPR [13,14] and optically detected magnetic resonance studies [9,15,16] have established a correlation between the Li_{Zn}^0 magnetic resonance line and a broad orange luminescence (OL) band with a maximum at 1.95 eV at 10 K [17–19]. The OL band is normally present in the photoluminescence (PL) spectrum of hydrothermally (HT) grown ZnO [18] crystals, which contain Li impurities with concentrations in the $(1–5) \times 10^{17}$ cm^{-3} range [20]. McNamara *et al.* [19] recently performed a detailed experimental analysis of the thermal quenching of the OL band in HT grown ZnO, and

obtained an ionization energy of 0.65 ± 0.10 eV for Li_{Zn}. The paramagnetic Na_{Zn}^0 state has similarly been observed by EPR and linked to a broad yellow luminescence (YL) band peaking at 2.18 eV at 50 K [21], but the concentration of Na impurities in HT grown ZnO is typically at least one order of magnitude lower than that of Li.

Holistic understanding of an extrinsic defect in a host semiconductor not only includes its behavior as an isolated defect, but its interplay with other important defects and impurities in the material. For instance, Li_{Zn} is known to form defect complexes with donor impurities in ZnO. Notable examples include: (i) $Li_{Zn}H$, which has been assigned to an infrared (IR) absorption line at 3577 cm^{-1}, the dominant OH-related IR absorption line in HT grown ZnO [22], and (ii) $Li_{Zn}Fe_{Zn}$, which has been identified by means of high-frequency EPR and electron-nuclear double resonance spectroscopy [23]. Importantly, since Li and donor dopants, primarily Al and H, are the main impurities in HT grown ZnO, such defect complexes may influence, and even dominate, its electrical and optical properties. The behavior of such complexes is not fully understood and reports are scarce in the literature, but they are often assumed to be fully passivated with no charge-state transition levels within the band gap.

Concurrently, despite the large body of work on Li in ZnO, pertinent questions remain. For instance, a structured blue luminescence (BL) band with a zero phonon line (ZPL) at 3.05 eV has been observed in Li-doped ZnO under certain conditions, and attributed to a transition between a shallow donor and a Li-related shallow acceptor with an ionization energy of 300 meV [24–26]. The specific defect origin is unclear, but a transient shallow Li_{Zn} state [27,28], or a

———
[*]ymirkf@fys.uio.no

Li$_{\text{Zn}}$-H-Li$_{\text{Zn}}$ complex [24,25] has been suggested. Furthermore, the OL band in HT grown ZnO is normally overlapped by a broad green luminescence (GL) at its high energy side [19]. Broad GL is almost ubiquitous in the PL spectrum of ZnO. However, Reshchikov *et al.* [18,29] have reported specific bands labeled GL1 and GL2 which were observed exclusively in HT grown ZnO. Their defect origins have not been established, but, since a high Li content is the primary difference between HT grown and other forms of ZnO crystals, Li-related defects are reasonable suspects.

In this work we present results from hybrid functional calculations on the thermodynamic, electrical, and optical properties of the Li$_{\text{Zn}}$ and Na$_{\text{Zn}}$ acceptors, and their complexes with the common donor impurities Al$_{\text{Zn}}$ and H in ZnO. The results for Li$_{\text{Zn}}$ and Na$_{\text{Zn}}$ are found to be in good agreement with experimental data on the OL and YL bands. Interestingly, we find that also the complexes are electrically (and optically) active. This result is further supported by PL and secondary ion mass spectrometry (SIMS) data on a HT grown ZnO sample, before and after annealing in Zn ambient in order to lower the concentration of Li impurities in the sample.

II. METHODOLOGY

A. Computational details

First-principles calculations were performed using the projector augmented wave method [30,31] with the Heyd-Scuseria-Ernzerhof (HSE) [32] range-separated hybrid functional, as implemented in the VASP code [33].

Hybrid functionals satisfying the generalized Koopmans theorem (gKT) have generally been found to describe polaronic localization well [34–37]. For this reason, the HSE(α, ω) functional was parametrized by using two different approaches: (i) conventionally by adjusting the fraction of screened Hartree-Fock exchange α to 0.375 [38] in order to reproduce the experimental band gap of 3.44 eV [39], while keeping the screening parameter ω fixed to the standard value of 0.2 Å^{-1}, and (ii) tuning α and ω to both satisfy the gKT and reproduce the experimental band gap [37]. We employed the $(0/-)$ transition of polaronic acceptors (V_{Zn}, Li$_{\text{Zn}}$, and Na$_{\text{Zn}}$) to test the gKT. When testing the gKT, it is crucial that finite-size errors are minimized; detailed information on our testing procedure, finite-size corrections, and the supercell-size dependence of the gKT related quantities can be found in the Appendix. We find that the HSE(0.30, 0.05) functional complies with the gKT and reproduces the experimental band gap, whereas the HSE(0.375, 0.20) functional results in a non-Koopmans energy of about 0.1 eV. This energy is small, and may still contain a small finite-size error, which we have estimated based on supercell-size tests in the Appendix. Nevertheless, the difference in results obtained with the two approaches can, at the very least, serve as a proxy for the sensitivity of the results with respect to the choice of α and ω parameters.

Bulk lattice constants were optimized for each functional until the forces were smaller than 1 meV/Å; the resulting lattice parameters differ by merely 0.01 Å. Defect calculations were then performed using 96-atom supercells, a plane-wave basis set with an energy cutoff of 500 eV, and a special k point at $(\frac{1}{4}, \frac{1}{4}, \frac{1}{4})$ for integrations over the Brillouin zone [40]. Ionic relaxation of defects was performed until the forces were reduced to less than 5 meV/Å, and spin polarization was included. Defect formation energies and thermodynamic charge-state transition levels were calculated by following the well-established formalism described in Refs. [41,42]. For example, the formation energy of Li$_{\text{Zn}}$ is given by

$$E_f^q(\text{Li}_{\text{Zn}}) = E_{\text{tot}}^q(\text{Li}_{\text{Zn}}) - E_{\text{tot}}^{\text{bulk}} + \mu_{\text{Zn}} - \mu_{\text{Li}} + q\epsilon_F, \quad (1)$$

where $E_{\text{tot}}^q(\text{Li}_{\text{Zn}})$ and $E_{\text{tot}}^{\text{bulk}}$ denote the total energy of the defect-containing and bulk supercells, q is the charge state of the defect, μ_{Zn} and μ_{Li} are the chemical potentials of the removed Zn and added Li atom, and ϵ_F is the Fermi level position referenced to the bulk VBM. The chemical potential can vary between O-rich and Zn-rich conditions, where the upper limit of μ_O and μ_{Zn} is given by the total energy per atom of an O$_2$ molecule and metallic Zn, respectively, and the lower limit is governed by the thermodynamic stability condition $\Delta H^f(\text{ZnO}) = \mu_{\text{Zn}} + \mu_O$ [43], where $H^f(\text{ZnO})$ is the formation enthalpy of ZnO [44]. The chemical potential of impurities is similarly bound by the solubility-limiting phases, i.e., Al$_2$O$_3$, Li$_2$O, Na$_2$O, and H$_2$O/H$_2$. We present calculated formation energies under intermediate conditions, i.e., halfway between O-rich and Zn-rich conditions, as the extreme limits are not usually reached under realistic growth conditions [45]. For charged defects we adopt the anisotropic [46] Freysoldt, Neugebauer, and Van de Walle (FNV) correction scheme [47].

Optical transition energies were calculated by using the effective one-dimensional (1D) configuration coordinate (CC) model described in Refs. [42,48–50]. Full luminescence lines were also calculated, including vibronic coupling, by using the methodology outlined in Ref. [48]. The effective 1D CC model is a good approximation for defects exhibiting strong electron-phonon coupling (large Huang-Rhys factor) [48,49], which is the case for all defects studied in the present work. The potential energy surfaces (PESs) in the CC diagrams were calculated by linearly interpolating the ground-state structures of the defect in the initial and final charge state, and computing the energy in the range -1.5 to $1.5 \times \Delta Q$ with steps of $0.1 \times \Delta Q$, where ΔQ is the difference in CC of the structures. We have calculated the vibrational wave functions χ and overlap integrals $\langle \chi_{em} | \chi_{gn} \rangle$, where m and n are the vibrational levels of the excited (e) and ground (g) state, from solutions of the Schrödinger equation for the calculated PESs by using a finite-difference method, as implemented in CarrierCapture.jl [51].

B. Experimental details

Two $5 \times 5 \times 0.5$ mm^3 sized samples were cut from a wafer of HT grown ZnO purchased from the MTI Corporation (Richmond, CA). One sample was sealed in a quartz ampoule containing a piece of $\sim$99.9% pure Zn foil, and annealed in a tube furnace at 900 °C for 1 h.

A Cameca IMS7f secondary ion mass spectrometer equipped with a 10 keV O$_2^+$ primary ion beam source was used to measure concentration versus depth profiles of Li, Na, Al, Fe, and Cu impurities in the as-grown and thermally processed samples. Depth calibration was performed by measuring the

sputtered crater depths with a Dektak 8 stylus profilometer and assuming a constant erosion rate. Implanted reference samples were used to calibrate the impurity concentration, resulting in an uncertainty of less than 10% in concentration values.

Steady-state PL was excited using a cw He-Cd laser with a photon energy of 3.81 eV. The emission was collected by a microscope and directed to a fiberoptic spectrometer (HR4000 and USB4000 Ocean Optics). The sample was kept at a temperature of 10 K using a closed-cycle He refrigerator. The PL spectra were corrected for the spectral response of the measurement system. Because the annealing resulted in a build up of impurities at the sample surface (for depths <3 μm), PL was excited inside the sputtered crater formed during the SIMS measurement. All presented impurity concentration values are for the bulk region (for depths >3 μm).

III. RESULTS AND DISCUSSION

A. Formation energies, thermodynamic charge-state transition levels, and structures

Figure 1 shows the calculated formation energy of the acceptors (Li_{Zn} and Na_{Zn}), donors (Al_{Zn}, H_i, and H_O), and their complexes ($Li_{Zn}Al_{Zn}$, $Li_{Zn}H$, $Li_{Zn}H_O$, $Na_{Zn}Al_{Zn}$, $Na_{Zn}H$, and $Na_{Zn}H_O$) as a function of the Fermi level position under intermediate conditions. Interestingly, the results obtained using HSE(0.375, 0.20) and HSE(0.30, 0.05) are very similar; thermodynamic charge-state transition levels differ by 50 meV at most, as shown in Table I.

The isolated donor impurities are shallow, contributing to the commonly observed unintentional n-type conductivity in ZnO [52–55]. For the isolated Li_{Zn} and Na_{Zn} acceptors, we find that both exhibit a dual behavior, as first reported by Lany and Zunger [27,28] using a Koopmans corrected semilocal functional, and later by Sun *et al.* [56] using the HSE(0.375,

TABLE I. Fermi level position in eV of the thermodynamic charge-state transition levels with respect to the VBM for the isolated and donor-complexed acceptors, calculated using the HSE(0.30, 0.05) and HSE(0.375, 0.20) functionals.

Defect	Transition	HSE(0.375, 0.20)	HSE(0.30, 0.05)
Li_{Zn}	$(0/-)$	0.72	0.67
	$(+/0)$	0.04	0.02
$Li_{Zn}Al_{Zn}$	$(+/0)$	0.36	0.31
$Li_{Zn}H$	$(+/0)$	0.12	0.09
$Li_{Zn}H_O$	$(+/0)$	0.11	0.08
Na_{Zn}	$(0/-)$	0.71	0.68
$Na_{Zn}Al_{Zn}$	$(+/0)$	0.37	0.34
$Na_{Zn}H$	$(+/0)$	0.31	0.27
$Na_{Zn}H_O$	$(+/0)$	0.29	0.26

0.20) functional. In the negative charge state, the Li and Na atoms reside near the ideal Zn site with approximate tetrahedral local symmetry, and no localized defect states in the band gap [28]. In the neutral charge state, two distinct acceptor states can occur [27,28]: (i) a metastable shallow state, where the hole is bound in an anisotropically delocalized hostlike state [56], and (ii) a deep ground state, which can be reached through a sizable symmetry-breaking lattice distortion. As shown in Fig. 2, the hole is trapped in a polaronic state localized at one of the four O ions immediately adjacent to the Li^+ or Na^+ ion, in agreement with EPR spectroscopy data [2,12,21,57]. Note that, in the deep state, the Li^+ ion moves far away from the hole polaron, towards the tetrahedral interstitial site, whereas the larger Na^+ ion stays near the ideal Zn site. We shall focus on the deep polaronic state, as the shallow state is only metastable [27]. However, our results for the shallow state are in line with the previous reports [27,56].

As shown in Table I, the thermodynamic $(0/-)$ transition levels of Li_{Zn} and Na_{Zn} occur between 0.67–0.72 eV above the VBM. This is consistent with previous calculations for the deep polaronic state [7,8,27,34,56,58,59], and the experimental ionization energy of 0.65 ± 0.10 eV for the OL band [19]. For Li_{Zn}, a second hole polaron can be stabilized at a separate adjacent O ion [34]. However, the resulting thermodynamic $(+/0)$ level occurs merely 0.02–0.04 eV above the VBM, which is within the expected error bar of the finite-size correction [46].

Complexing Li_{Zn} or Na_{Zn} with a single donor results in a charge-compensated neutral pair. Contrary to common assumption, however, our calculations show that the complexes are not fully passivated, as they can be stabilized in the positive charge state for Fermi level positions close to the VBM, making them exceedingly deep donors. Figure 2 shows the relaxed structure of four representative complexes; the positive charge state corresponds to a hole polaron localized at an adjacent O ion, similar to the charge-neutral isolated acceptors. The resulting thermodynamic $(+/0)$ transition levels are provided in Table I and occur between 0.08–0.37 eV above the VBM.

Interestingly, the complexes involving Al_{Zn} and H_i have very low formation energies (regardless of the chemical potential), which indicates that a sizable equilibrium
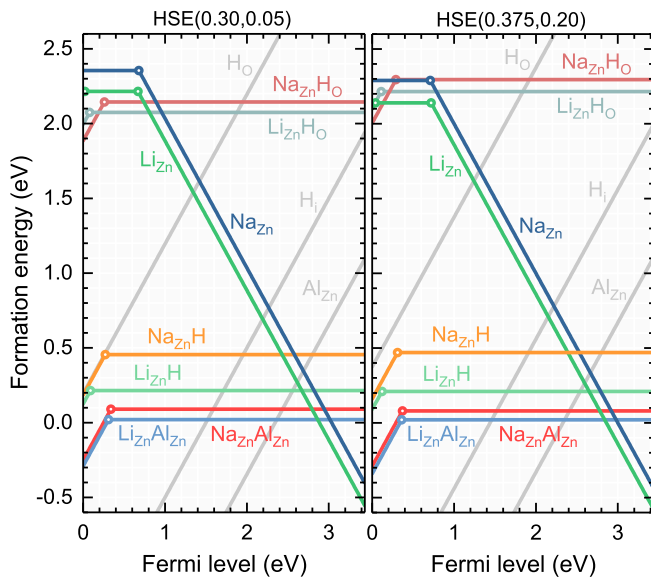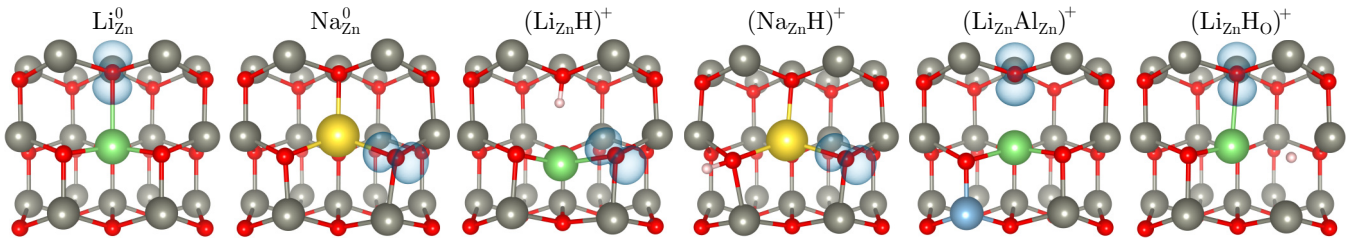

FIG. 1. Formation energy of the donors, acceptors, and their complexes as a function of the Fermi level position relative to the VBM under intermediate conditions, calculated using the HSE(0.30, 0.05) and HSE(0.375, 0.20) functionals.

FIG. 2. Relaxed structure of Li_{Zn}^0 with the hole (blue isosurface, set at $6 \times 10^{-3} r_{Bohr}^{-3}$) trapped in a polaronic state at the axial O ion, Na_{Zn}^0 with the hole trapped at one of the three azimuthal O ions, and four complexes with H and Al_{Zn} donors.

concentration can be expected when these impurities are incorporated during growth. They are particularly likely to form under compensated growth conditions, i.e., when the Fermi level is pinned close to the crossing point between the formation energy of Li_{Zn} or Na_{Zn} and a donor impurity, as the calculated formation energy of the defect complex is then lower than that of both constituents [60]. HT grown ZnO samples are typically compensated, and so a large fraction of the Li_{Zn} and Na_{Zn} acceptors can be expected to be complexed with donor impurities [22]. The complexes involving H_O exhibit rather high formation energies under intermediate conditions. Under Zn-rich conditions, however, their formation energies ($\sim$0.6 eV) are comparable to the other complexes.

In order to assess the stability of the defect complexes, we have also calculated removal energies by taking the difference in formation energy between the defect complex and the two remaining entities (in their most stable configuration) when the donor impurity is removed (calculated using separate supercells for each defect). The sign is chosen such that a positive removal energy corresponds to a stable complex. All of the studied complexes are found to be stable, with removal energies of 0.52, 1.17, 1.01, 0.60, 1.08, and 1.09 eV for $Li_{Zn}Al_{Zn}$, $Li_{Zn}H$, $Li_{Zn}H_O$, $Na_{Zn}Al_{Zn}$, $Na_{Zn}H$, and $Na_{Zn}H_O$, respectively.

For $Li_{Zn}H$ and $Na_{Zn}H$, we find that H prefers the bond-centered axial and antibonding azimuthal site, respectively, as shown in Fig. 2. This is consistent with IR absorption data [22] and previous local density functional calculations by Wardle *et al.* [6]. Investigations on the thermal stability of the $Li_{Zn}H$ complex via the IR absorption line at 3577 cm^{-1} has led to conflicting results in the literature [61–63]. In some samples, it starts to disappear at temperatures exceeding about 500 °C, while in others it can withstand heat treatments up to around 1200 °C [61–63]. The dissociation temperature for the $Li_{Zn}H$ complex can be estimated based on an activated process with a jump rate given by $\Gamma = \Gamma_0 \exp(-E_a/k_B T)$ [43,64]. Here the activation energy (E_a) is taken as the sum of the calculated removal energy of $Li_{Zn}H$ (1.17 eV) and the experimental migration barrier of H_i (0.85 ± 0.19 eV [65]). The attempt frequency (Γ_0) is set to a typical phonon frequency of 10 THz, and the jump rate at which dissociation starts to occur is assumed to be 1 Hz [64]. The resulting dissociation temperature is 510 ± 75 °C, consistent with the lower experimental temperature of 500 °C. It has been suggested that an apparent stability up to 1200 °C is due to retrapping of H_i^+ by Li_{Zn}^- [61–63].

For $Li_{Zn}Al_{Zn}$ and $Na_{Zn}Al_{Zn}$, there are three symmetrically inequivalent configurations for the donor. Kutin *et al.* [23]

observed all three configurations of the analogous $Li_{Zn}Fe_{Zn}$ complex. We have explored configurations with the donor located on the opposite side from the hole polaron (Fig. 2). We have also explored the analogous complexes with Fe_{Zn} or Ga_{Zn} [66] replacing Al_{Zn}, but these were found to be almost identical in terms of removal energy and position of the $(+/0)$ transition level. Al is also the most common of these impurities; the concentration of Al in as-grown ZnO usually varies between 10^{15} and 10^{17} cm^{-3} for different growth techniques [55]. For these reasons, we have presented results only for Al_{Zn}.

For $Li_{Zn}H_O$ and $Na_{Zn}H_O$, we find that the differences in energy between the axial and azimuthal H_O configurations are negligible. Hence, we present results for only the azimuthal configuration of H_O, as shown in Fig. 2.

B. Optical transitions and luminescence lines

We begin by examining the optical properties of the isolated Li_{Zn} and Na_{Zn} acceptors, and comparing the results with experimental data on the OL and YL bands. Figure 3 shows calculated CC diagrams for optical electron transitions between the CBM and the $(0/-)$ transition levels of Li_{Zn} and Na_{Zn}. The vertical axis in the CC diagrams corresponds to the transition energy, and the horizontal axis corresponds to the configuration coordinate (Q) which is a 1D parametrization of the collective motion of all atoms in the supercell between the two different charge states [42,67]. The ground state PES represents the negatively charged acceptor, and the excited state PES represents the neutral acceptor plus an electron at the CBM. The two PESs are vertically displaced by the energy difference between the thermodynamic $(0/-)$ transition level and the CBM, which is commonly referred to as the zero phonon line energy (E_{ZPL}). In the Franck-Condon approximation, optical transitions take place without atomic motion and are thus vertical in the CC diagrams, and the transition energies E_{em} and E_{abs} correspond approximately to the peak of the emission and absorption spectrum [42]. After emission, the defect will relax to its equilibrium atomic configuration, losing the Franck-Condon relaxation energy (d_g^{FC}).

The Li_{Zn} and Na_{Zn} acceptors exhibit similar polaronic defect states, and the positions of their thermodynamic $(0/-)$ levels are close, but there are clear differences in their CC diagrams. Strikingly, the ground-state PES of Li_{Zn} is strongly anharmonic compared to Na_{Zn} [59], and the value of d_g^{FC} is about 0.2 eV larger for Li_{Zn}, while the CC diagram for Na_{Zn} calculated using HSE(0.375, 0.20) is similar to those calculated previously for V_{Zn}-related defects in ZnO [44,45,50].
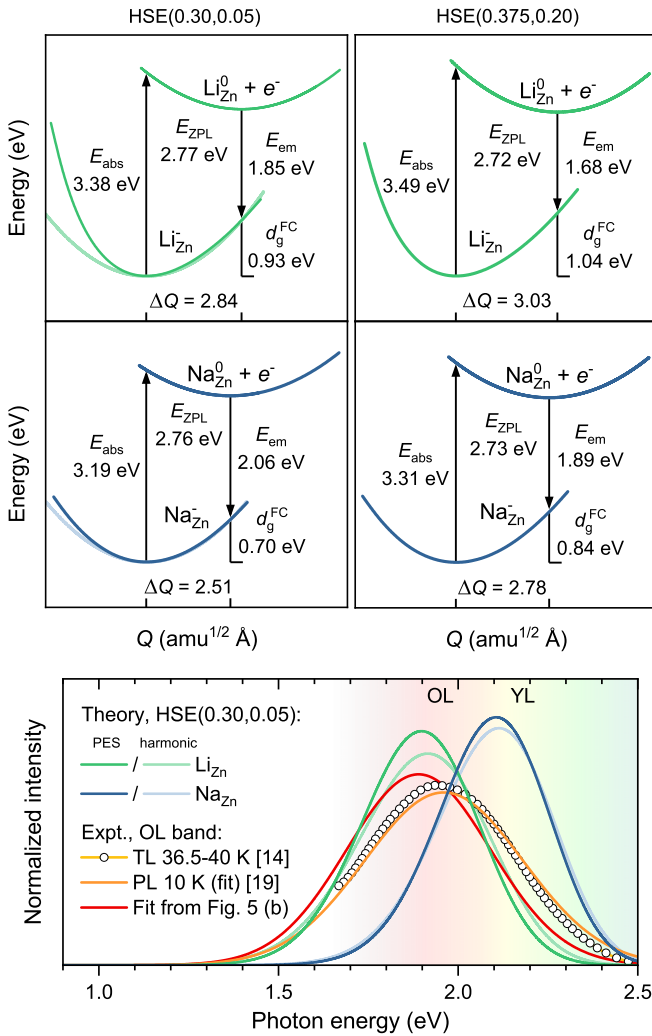
FIG. 3. Top panels: CC diagrams for optical electron transitions between the CBM and the $(0/-)$ levels of Li_{Zn} and Na_{Zn}, calculated using HSE(0.375, 0.20) and HSE(0.30, 0.05). Bottom panel: Luminescence lines of Li_{Zn} and Na_{Zn} calculated for the HSE(0.30, 0.05) CC diagram using both the computed PES and harmonic approximation (the parabolas shown in the CC diagrams). Experimental data for the OL band from Refs. [14,19] is included for comparison. Experimental OL and YL band labels are positioned at their peak positions.

This difference is caused by the aforementioned large displacement of the Li^+ ion upon hole capture by the acceptor. The resulting difference in E_{em} for Li_{Zn} and Na_{Zn} (about 0.2 eV) is consistent with the difference in peak position of the experimental OL and YL bands (0.23 eV) [18,21]. Comparing the two different functionals, both the magnitude of the total mass-weighted distortion (ΔQ) and d_g^{FC} is lowered when using HSE(0.30, 0.05) compared to HSE(0.375, 0.20). Moreover, the differences in E_{em} are larger than those in E_{ZPL}.

The calculated E_{abs} values for Li_{Zn} (3.38–3.49 eV) are consistent with photo-EPR experiments by Nikitenko [68], where the absorption spectrum related to the optically induced EPR signal of Li_{Zn} was measured to peak at about 3.25 eV. When using the HSE(0.375, 0.20) functional, the calculated emission energies of Li_{Zn} (1.68 eV) and Na_{Zn} (1.89 eV) are

underestimated by about 0.3 eV relative to the peak positions of the experimentally observed OL (1.95 eV at 10 K [18]) and YL (2.18 eV at 50 K [21]) bands. When HSE(0.30, 0.05) is used, the calculated emission energies for Li_{Zn} (1.85 eV) and Na_{Zn} (2.06 eV) are both shifted up in energy by 0.17 eV. Thus, assuming that the OL and YL bands are indeed caused by electron transitions between the CBM and the $(0/-)$ levels of Li_{Zn} and Na_{Zn}, the HSE(0.30, 0.05) functional appears to provide the most accurate description of Li_{Zn} and Na_{Zn}. However, both approaches yield results that agree reasonably well with the experimental data.

Figure 3 also shows the luminescence lines calculated for the CC diagrams obtained using the HSE(0.30, 0.05) functional. When using HSE(0.375, 0.20), the line shapes are similar, but the peak positions are lower in energy. Experimental data is also included in Fig. 3; specifically, the thermoluminescence (TL) band reported by Zwingel [14], the Gaussian curve fit to the OL band in HT grown ZnO reported by McNamara *et al.* [19], and the Gaussian curve fit to the OL band observed in the annealed sample in the present work. In order to assess the impact of the anharmonic PES of Li_{Zn} on the line shape, the line shapes were calculated both for the computed PES and a parabola intersecting the relaxation energy (harmonic approximation). The calculated Li_{Zn} luminescence line peaks at 1.90 eV and has a full-width at half-maximum (FWHM) of 0.39 eV (0.43 eV for the harmonic line shape), which is lower than the experimental FWHM of about 0.5 eV for the OL band [14,18,19]. Optical transitions involving both axial and azimuthal hole configurations are likely to occur, since both are observed by EPR, which could broaden the overall line shape. However, we find that the azimuthal peak position is only 20 meV higher in energy than the axial one, and the line shapes are almost identical. The Na_{Zn} luminescence line associated with the azimuthal hole configuration peaks at 2.11 eV and has a FWHM of 0.36 eV (0.38 eV for the harmonic line shape), whereas the axial one peaks 40 meV higher in energy with a similar line shape. This is in better agreement with experimental data; Zwingel and Gärtner [21] reported a FWHM of 0.4 eV for the YL band at 50 K (TL), but no spectrum was shown.

The emergence of $(+/0)$ transition levels for the defect complexes has important consequences for their optical properties, as they can potentially give rise to broad luminescence bands. In fact, similar predictions have been made to explain the luminescence bands related to isolated and donor-complexed C_N acceptors in GaN [69–72].

Calculated CC diagrams for optical transitions involving the CBM and the $(+/0)$ transition level of the complexes are shown in Fig. 4. The emission energies of the complexes are blueshifted with respect to those of the isolated acceptors, which makes the complexes candidates for the defect origin of the broad GL in HT grown ZnO. Interestingly, $Li_{Zn}Al_{Zn}$ and $Li_{Zn}H_O$ retain the anharmonicity exhibited by Li_{Zn} for the ground-state PES, while $Li_{Zn}H$ does not. This can be understood from the structure of the $Li_{Zn}H$ complex. The H atom pins the Li^+ ion near the tetrahedral interstitial site (see Fig. 2), and thus Li^+ does not undergo the large displacement along the direction of the axial Li-O bond upon hole capture. Figure 4 shows the calculated luminescence lines for the complexes. Their FWHM values are about 0.37 eV (except for the
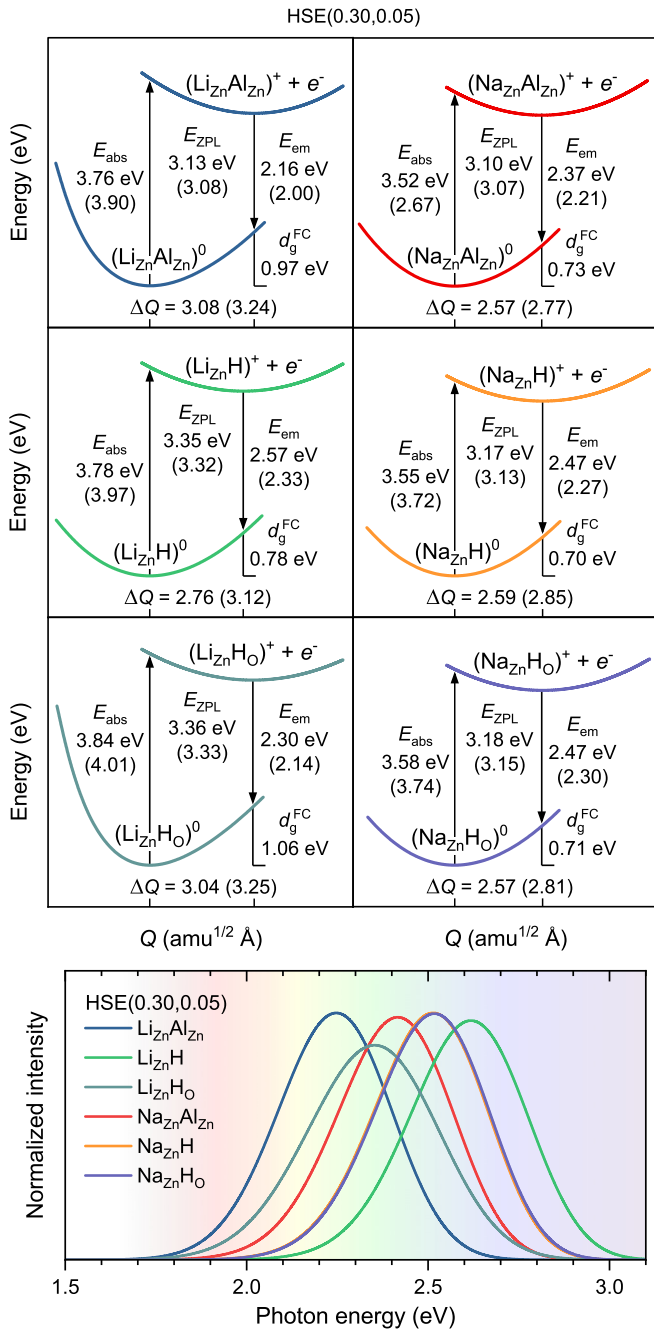
FIG. 4. Top panels: CC diagrams for optical electron transitions between the CBM and the (+/0) transition level of donor-complexed Li_{Zn} and Na_{Zn} acceptors, calculated using HSE(0.30, 0.05). The corresponding values of E_{abs}, E_{ZPL}, E_{em}, and ΔQ calculated using HSE(0.375, 0.20) are given in parentheses. Bottom panel: Corresponding luminescence lines of $Li_{Zn}Al_{Zn}$, $Li_{Zn}H$, $Li_{Zn}H_O$ $Na_{Zn}Al_{Zn}$, $Na_{Zn}H$, and $Li_{Zn}H_O$.

$Li_{Zn}H_O$ line which has a FWHM of 0.42 eV). These values are similar to those obtained for the isolated acceptors, which is reasonable because the charge-state transitions occur through the same type of polaronic state with similar magnitudes of ΔQ.

Since all the calculated luminescence lines have similar shapes and peak positions, distinguishing them experimen-

tally could be challenging, especially for the different complexes. It might be possible to discern between isolated and donor-complexed acceptors based on other band characteristics, e.g., carrier capture coefficients, lifetime, and temperature dependence. However, it should be noted that, since the broad luminescence band observed in HT grown ZnO consists of several overlapping bands, obtaining accurate and reliable data for these other band characteristics is also challenging. Thus, a detailed comparison between PL measurements and theory for these properties is beyond the scope of the present work. Qualitatively, however, some differences could be expected between the isolated and donor-complexed acceptors. Indeed, the (+/0) levels of the complexes are positioned very close to the VBM, which means that luminescence bands related to the complexes should exhibit lower activation energies of thermal quenching. This is consistent with the GL2 band in HT ZnO reported by Reshchikov *et al.* [18], where GL2 starts to quench at 40 K with a low activation energy of 35 meV.

Furthermore, the OL band in ZnO is characterized by a large hole capture coefficient [72,73]; in the limit of low excitation intensity, the OL band dominates the PL spectrum from HT grown ZnO [29,74]. This is due to the low barrier for nonradiative hole capture by Li_{Zn}^-, and its attractive Coulomb interaction with photogenerated holes [59,72]. The subsequent radiative electron capture, however, is slow because Li_{Zn}^0 is charge neutral in the excited state [18,29,72]. For transitions involving the (+/0) levels of the complexes, however, an opposite behavior can be anticipated [72]. Since the defect complexes are initially charge neutral, they will capture photogenerated holes slowly compared to isolated acceptors [59,72]. The subsequent radiative electron capture, however, will take place rapidly as now the complexes are positively charged. The positively charged complexes will also have a hydrogenic effective-mass state very close to the CBM, which could behave as a so-called giant trap for nonradiative electron capture [71,72,75]. This is consistent with the GL2 band, which exhibits fast and exponential decay after pulse excitation [18], while the OL band exhibits slow and nonexponential decay [29,75].

Finally, Demchenko *et al.* [71,72] have suggested that the $C_N H$ complex in GaN gives rise to a broad BL band, which, upon ultraviolet light exposure, gradually dissociates and leaves behind a broad YL band (C_N) [71,72]. The calculated removal energy for $C_N H$ in Ref. [71] is similar to the ones we obtain for the $Li_{Zn}H$ and $Na_{Zn}H$ complexes, and the H configuration is the same as the one we obtain for $Na_{Zn}H$. Hence, the luminescence bands originating from $Li_{Zn}H$ and $Na_{Zn}H$ complexes might also bleach under prolonged ultraviolet light exposure. Indeed, a similar GL band has been observed in melt-grown ZnO, which bleached and gave way to a YL band [76].

C. Experimental PL and SIMS results

Figure 5 shows PL spectra of the as-grown and annealed HT grown ZnO samples. Here we will focus mainly on the broad luminescence band that extends from about 1.5 to 2.9 eV. We find that the temperature and excitation power dependence of this band in the as-grown sample is similar
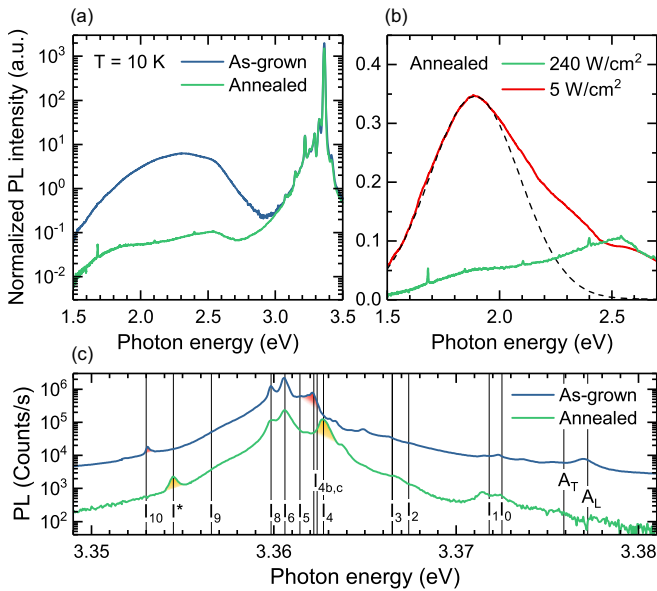
FIG. 5. Normalized PL spectrum (divided by excitation power) of (a) the as-grown and annealed ZnO samples, and (b) deep level emission of the annealed sample with high and low excitation power density. The dashed line is a Gaussian curve fit peaking at 1.89 eV with a FWHM of 0.47 eV. (c) Near band edge emission of the as-grown and annealed samples. Free and donor-bound exciton lines are indicated (labels and energy positions are taken from Refs. [9,77]), and those that are discussed in the text have been highlighted.

to what has been described in detail previously for several HT grown ZnO samples by Reshchikov *et al.* [18,29,73] and McNamara *et al.* [19]. As already mentioned, the OL band (Li_{Zn}) dominates in the limit of low excitation power (see, e.g., Fig. 3 in Ref. [74]). As the excitation power is increased, the band maximum gradually shifts up in energy, i.e., the OL saturates and the GL grows [29]. In Fig. 5 the overall band maximum is at about 2.3 eV for the as-grown sample.

The concentration of Li_{Zn}-related defects can be lowered significantly via thermal processing in reducing (Zn-vapor) atmosphere, as in-diffusing Zn_i can convert immobile Li_{Zn} acceptors into highly mobile Li_i donors [3,7,78–80]. Thus, if donor-complexed Li_{Zn} acceptors are responsible for the broad GL at the high energy side of the OL band, then the entire broad luminescence band should be strongly suppressed following such thermal treatment.

Table II lists the bulk concentration of Li, Na, and Al impurities in the as-grown and annealed ZnO samples. Annealing in Zn ambient causes the Li concentration to drop from 2×10^{17} to 2×10^{14} cm^{-3}, while the concentration of

TABLE II. Bulk concentration of impurities in the as-grown and annealed samples determined using SIMS. The concentration of Fe, Si, and Cu is below the detection limit.

Element	As-grown (cm^{-3})	Annealed (cm^{-3})
Li	2×10^{17}	2×10^{14}
Na	2×10^{15}	2×10^{15}
Al	8×10^{16}	8×10^{16}

Na and Al remains unchanged. Al is the dominant donor impurity, whereas the concentration of Fe and Si is below the respective SIMS detection limits for these elements. H is likely present as well, albeit with a concentration below the SIMS detection limit of $\sim 5 \times 10^{17}$ cm^{-3}. The concentration of Cu is below the SIMS detection limit in both samples, which is important because the Cu_{Zn} acceptor in ZnO has been assigned to a structured GL band peaking at 2.45 eV [74,81,82] that can interfere with the analysis of overlapping bands. We did not observe this structured GL band in the PL spectrum of the as-grown or annealed samples.

As shown in Fig. 5(a), annealing the sample in Zn ambient causes a dramatic decrease in the intensity of the entire broad luminescence band. This suggests that Li is involved not only in the OL band, but also in the GL at its high energy side. Indeed, the SIMS results show a strong depletion of Li, while the concentration of other impurities is unaffected. The remaining broad luminescence appears to consist of two main bands. As shown in Fig. 5(b), the lower energy band dominates when the excitation power is lowered, similar to the as-grown sample, which may indicate that this is the OL band. The low energy band can be fitted to a Gaussian with a peak position of 1.89 eV and FWHM of 0.47 eV, which is close to the values for the OL band [19].

It should be noted that the SIMS data does not provide any information about the configuration of the impurities, e.g., the fraction of isolated to complexed Li_{Zn} and Na_{Zn} acceptors. Furthermore, the present experimental results cannot rule out intrinsic defects. As an example, the GL could be caused by V_{Zn}-donor complexes [50], the concentration of which would also drop following heat treatment in Zn ambient. However, the concentration of Li is expected to be higher than that of V_{Zn}-related defects in as-grown HT ZnO [83]. In addition, previous hybrid functional calculations show that the only V_{Zn}-donor complexes that can give rise to GL bands are positively charged in the ground state [50], which means that capture of photogenerated holes will be very inefficient compared to the Li_{Zn}-related defects studied here. Finally, the GL1 and GL2 bands were observed exclusively in HT grown ZnO [18,29], which favors extrinsic Li- over intrinsic V_{Zn}-related defects.

Removal of Li from Li_{Zn}-donor complexes upon annealing is also evidenced by changes in the intensity of neutral donor-bound exciton (D_0X) lines in the PL spectrum. Figure 5(c) shows the near band edge emission in the as-grown and annealed samples, with exciton lines indicated. The labels and energies of the exciton lines were taken from Refs. [9,77]. The D_0X line associated with H_O (I_4) is commonly observed in ZnO [84], but is absent in the as-grown sample. This is consistent with the recent study by Heinhold *et al.* [77], where the I_4 line was replaced by two closely lying D_0X lines labeled $I_{4b,c}$ in HT grown ZnO. These lines were observed exclusively in HT grown ZnO, and were therefore assigned to donors involving the $Li_{Zn}H_O$ complex plus an additional donor (possibly $Li_{Zn}H$-H_O). We also observe the $I_{4b,c}$ lines in the as-grown sample (albeit as a single peak due to a lower resolution). After lowering the Li concentration via annealing, the $I_{4b,c}$ line disappears while I_4 appears, supporting the assignment by Heinhold *et al.* [77], i.e., indiffusing Zn_i converts $Li_{Zn}H_O$ into H_O. Similarly, the I_{10} line is present only in

the as-grown sample. Isotope substitution experiments have demonstrated that I_{10} is related to Sn, and a $Sn_{Zn}Li_{Zn}$ complex has been suggested [85]. This assignment is supported by the present results, as the I_{10} line disappears after annealing.

Finally, a line labeled I^* appears at 3.3545 eV after annealing the sample. To our knowledge, there is no defect assignment for this line in the literature. If the responsible defect is a donor, its donor binding energy (E_D) can be estimated from the localization energy (E_{loc}) with reference to the transverse free-exciton ($A_T = 3.3754$ eV) by using Haynes rule [86] with coefficients from Ref. [77], i.e., $E_{loc} = 0.34E_D - 2.71$ meV. The resulting donor binding energy is 69.4 meV. If I^* is of D_0X nature, one would expect to observe a two-electron satellite signature in the spectral range 3.3024–3.3036 eV [9], but no such signature was observed in this region. However, this does not necessarily disprove a D_0X origin. A neutral acceptor-bound exciton (A_0X) origin has also been suggested for lines observed in this region [9,25,87]. Using Haynes rule for acceptors [88–90], the estimated acceptor binding energy would then be in the range 140–210 meV.

IV. CONCLUSION

Using hybrid functional calculations, we have investigated Li_{Zn} and Na_{Zn} acceptors, and their complexes with common shallow donor impurities Al_{Zn} and H_i in ZnO. The complexes have low formation energies, regardless of the chemical potential, which means that a sizable equilibrium concentration can be expected when these impurities are incorporated during materials growth, especially under highly compensated growth conditions.

Interestingly, our calculations show that the $Li_{Zn}Al_{Zn}$, $Li_{Zn}H$, $Na_{Zn}Al_{Zn}$, and $Na_{Zn}H$ complexes can be stabilized in the positive charge state, resulting in thermodynamic $(+/0)$ transition levels located between 90–370 meV above the VBM. By employing an effective 1D CC model, we predict that these complexes can give rise to broad luminescence bands peaking at the high energy side of the OL (Li_{Zn}) [18] and YL (Na_{Zn}) [21] bands. Since the luminescence bands are similar in shape and position, careful analysis of PL data will be crucial in order to pinpoint specific defects. The overall picture is similar to what has been found previously for the C_N acceptor and its complexes with donors in GaN [69–72].

Following heat treatment in Zn ambient, the concentration of Li in HT grown ZnO is lowered by about three orders of magnitude, while the concentration of Na and Al remains basically unchanged. The change in Li concentration is accompanied by a strong reduction in intensity of the entire broad luminescence band, which may suggest that Li is involved not only in the OL band, but also in the broad GL at its high energy side, with donor-complexed Li_{Zn} and Na_{Zn} as a potential origin. However, further work is required in order to verify this hypothesis.

TABLE III. Calculated non-Koopmans energies in eV for the $(0/-)$ transition of polaronic acceptors V_{Zn}, Li_{Zn}, and Na_{Zn}, and the $(+/0)$ transition of H_i at the octahedral site.

Defect	Transition	E_{NK} (eV)	
		HSE(0.375, 0.20)	HSE(0.30, 0.05)
V_{Zn}	$(0/-)$	0.08	−0.01
Li_{Zn}	$(0/-)$	0.06	0.01
Na_{Zn}	$(0/-)$	0.07	0.00
H_i	$(+/0)$	0.27	0.07

APPENDIX

Here we discuss the gKT fitting procedure and the supercell-size dependence of gKT related quantities. The gKT is an exact physical constraint by which the total energy shows a piecewise linear dependence upon addition of electrons, and implies that the single-particle energy level does not shift upon occupation [34,35,91]. To determine whether the gKT is fulfilled, we have used the $(0/-)$ transition of the unrelaxed V_{Zn} and calculated the so-called non-Koopmans energy, which is given by [34]

$$E_{NK} = E_{add} - \varepsilon(N). \tag{A1}$$

Here $\varepsilon(N)$ is the KS eigenvalue of the defect state in the neutral charge state (N-electron system), and $E_{add} = E(N + 1) - E(N)$ is the electron addition energy, i.e., the total en-
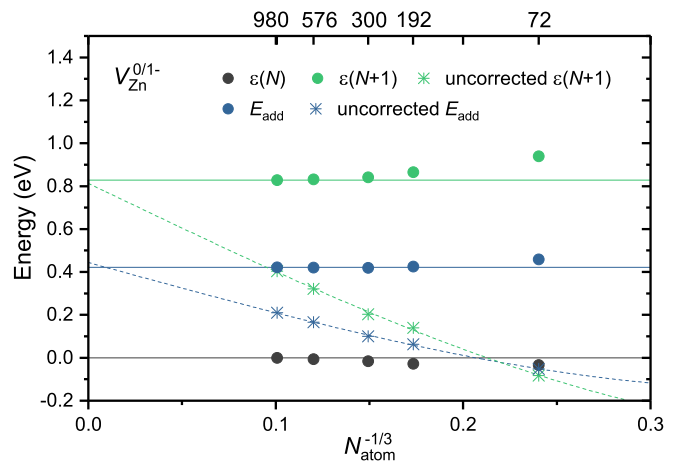

FIG. 6. Dependence of corrected and uncorrected gKT quantities on supercell size for the $(0/-)$ transition of the unrelaxed V_{Zn} in ZnO using the GGA-PBE+U functional, where an effective U value of 5 eV was applied to the Zn $3d$ orbitals, and 8 eV to the O $2p$ orbitals of the four O atoms associated with V_{Zn}. A Γ-only k-point sampling was used for all supercells. N_{atom} is the number of atoms in the supercell. The energy is given relative to the $\varepsilon(N)$ value of the largest supercell. The dashed lines are fits of the uncorrected values to a function of the form $aN_{atom}^{-1} + bN_{atom}^{-1/3} + c$, and the solid lines correspond to the value obtained for the largest supercell.
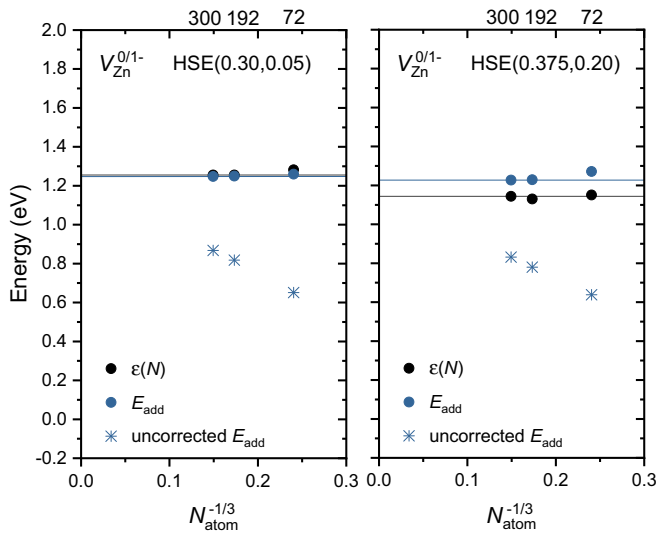
FIG. 7. Dependence of corrected and uncorrected gKT quantities on supercell size for the $(0/-)$ transition of the unrelaxed V_{Zn} in ZnO using HSE(0.30, 0.05) and HSE(0.375, 0.20).

ergy difference between the N- and $(N+1)$-electron systems, keeping the atoms fixed. The finite-size correction [46,47] for charged defects was applied to the terms pertaining to the negatively charged supercell, namely $E(N+1)$ and $\varepsilon(N+1)$, using the ion-clamped dielectric tensor. For KS eigenvalues, the correction is given by the relation $\varepsilon_c = -2E_c/q$ [92], where q is the charge state and E_c is the total energy correction. When $E_{NK} = 0$, the gKT is fulfilled as $e_N = E_{add} = e_{N+1}$, i.e., the KS eigenvalue does not shift upon occupation.

The test was carried out by using a 300-atom supercell and a Γ-only k-point sampling, which is the largest supercell we could afford. For each set of α and μ parameters tested, the bulk lattice parameters were optimized, and the ion-clamped dielectric tensor calculated from the self-consistent response of the system to a finite electric field [93]. As shown in Table III, we obtain $E_{NK} = 0.08$ eV for the $(0/-)$ transition of V_{Zn} when using the HSE(0.375, 0.20) functional, which means that the defect KS eigenvalue shifts upward in energy upon electron addition. By systematically changing the μ and α parameters and calculating E_{NK}, we find that the HSE(0.30,

0.05) functional both satisfies the gKT for V_{Zn} and reproduces the experimental band gap.

We have calculated E_{NK} also for the $(0/-)$ transitions of Li_{Zn} and Na_{Zn}, and the $(+/0)$ transition of H_i with the H atom at the octahedral interstitial site [35]. For Li_{Zn} and Na_{Zn}, however, there is a caveat, because the acceptor state is delocalized when the Li/Na atom is placed at the ideal Zn site, making it unsuitable for gKT testing [35,36]. Instead, we have shifted the Li/Na atom to the O basal plane. This results in a well-localized defect state for both charge states, similar to the defect states shown in Fig. 2. The resulting E_{NK} values for Li_{Zn} and Na_{Zn} are consistent with those obtained for V_{Zn} in Table III, and the HSE(0.30, 0.05) functional satisfies the gKT approximately. For H_i, the calculated E_{NK} is larger and seems to be more sensitive to the α and μ parameters. This result is in line with the trend observed by Miceli *et al.* [35]. The reason for the discrepancy could be due to the different character of the H_i defect state, or a larger remaining finite-size error. The latter can be expected due the more extended nature of the H_i defect state. In any case, the HSE(0.30, 0.05) functional is found to satisfy the gKT for polaronic O $2p$-like states, which is the type of defect state investigated in the present work.

Although we have not explored the entire α and ω parameter space, we find that other sets of parameters that comply with the gKT tend to produce similar band gap values, in line with results reported by Miceli *et al.* [35]. For instance, HSE(0.40, 0.20) results in $E_{NK} = -0.01$ eV for V_{Zn} and a band gap of 3.58 eV.

Finally, to investigate the supercell-size dependence of the calculated gKT quantities for V_{Zn}, we have performed a test using the PBE-GGA+U functional. As shown in Fig. 6, the KS defect state shifts up after electron addition, and E_{add} is located at an average between $\varepsilon(N)$ and $\varepsilon(N+1)$ [36]. E_{NK} in the 300-atom supercell is within 13 meV of the value calculated for the largest 980-atom supercell, and, as indicated by the solid and dashed lines in Fig. 6, the terms pertaining to the singly negatively charged supercell are well corrected by the FNV scheme. The supercell-size dependence was also investigated up to the 300-atom supercell using the HSE(0.30, 0.05) and HSE(0.375, 0.20) functionals, as shown in Fig. 7. When using the HSE functionals, E_{NK} converges even faster.

[1] J. Lander, J. Phys. Chem. Solids. **15**, 324 (1960).

[2] J. Schneider and O. Schirmer, Z. Naturforsch. Teil A **18**, 20 (1963).

[3] P. T. Neuvonen, L. Vines, A. Y. Kuznetsov, B. G. Svensson, X. Du, F. Tuomisto, and A. Hallén, Appl. Phys. Lett. **95**, 242111 (2009).

[4] C. H. Park, S. B. Zhang, and S.-H. Wei, Phys. Rev. B **66**, 073202 (2002).

[5] S. B. Orlinskii, J. Schmidt, P. G. Baranov, D. M. Hofmann, C. de Mello Donegá, and A. Meijerink, Phys. Rev. Lett. **92**, 047603 (2004).

[6] M. G. Wardle, J. P. Goss, and P. R. Briddon, Phys. Rev. B **71**, 155205 (2005).

[7] A. Carvalho, A. Alkauskas, A. Pasquarello, A. K. Tagantsev, and N. Setter, Phys. Rev. B **80**, 195205 (2009).

[8] T. S. Bjørheim, S. Erdal, K. M. Johansen, K. E. Knutsen, and T. Norby, J. Phys. Chem. C **116**, 23764 (2012).

[9] B. K. Meyer, H. Alves, D. M. Hofmann, W. Kriegseis, D. Forster, F. Bertram, J. Christen, A. Hoffmann, M. Straßburg, M. Dworzak, U. Haboeck, and A. V. Rodina, Phys. Status Solidi B **241**, 231 (2004).

[10] M. D. McCluskey, C. D. Corolewski, J. Lv, M. C. Tarun, S. T. Teklemichael, E. D. Walter, M. G. Norton, K. W. Harrison, and S. Ha, J. Appl. Phys. **117**, 112802 (2015).

[11] P. H. Kasai, Phys. Rev. **130**, 989 (1963).

[12] O. Schirmer, J. Phys. Chem. Solids **29**, 1407 (1968).

[13] O. Schirmer and D. Zwingel, Solid State Commun. **8**, 1559 (1970).

[14] D. Zwingel, J. Lumin. **5**, 385 (1972).

[15] R. Cox, D. Block, A. Hervé, R. Picard, C. Santier, and R. Helbig, Solid State Commun. **25**, 77 (1978).

[16] R. Laiho, L. S. Vlasenko, and M. P. Vlasenko, J. Appl. Phys. **103**, 123709 (2008).

[17] M. A. Reshchikov, J. Garbus, G. Lopez, M. Ruchala, B. Nemeth, and J. Nause, Mater. Res. Soc. Symp. Proc. **957**, K07-19 (2006).

[18] M. Reshchikov, H. Morkoç, B. Nemeth, J. Nause, J. Xie, B. Hertog, and A. Osinsky, Phys. B Condens. Matter **401–402**, 358 (2007).

[19] J. McNamara, N. Albarakati, and M. Reshchikov, J. Lumin. **178**, 301 (2016).

[20] L. Vines, E. V. Monakhov, R. Schifano, W. Mtangi, F. D. Auret, and B. G. Svensson, J. Appl. Phys. **107**, 103707 (2010).

[21] D. Zwingel and F. Gärtner, Solid State Commun. **14**, 45 (1974).

[22] L. E. Halliburton, L. Wang, L. Bai, N. Y. Garces, N. C. Giles, M. J. Callahan, and B. Wang, J. Appl. Phys. **96**, 7168 (2004).

[23] Y. Kutin, G. Mamin, and S. Orlinskii, J. Magn. Reson. **237**, 110 (2013).

[24] J. Sann, A. Hofstaetter, D. Pfisterer, J. Stehr, and B. K. Meyer, Phys. Status Solidi C **3**, 952 (2006).

[25] B. K. Meyer, J. Stehr, A. Hofstaetter, N. Volbers, A. Zeuner, and J. Sann, Appl. Phys. A **88**, 119 (2007).

[26] Z. Zhang, K. E. Knutsen, T. Merz, A. Y. Kuznetsov, B. G. Svensson, and L. J. Brillson, Appl. Phys. Lett. **100**, 042107 (2012).

[27] S. Lany and A. Zunger, Appl. Phys. Lett **96**, 142114 (2010).

[28] S. Lany, Phys. Status Solidi B **248**, 1052 (2011).

[29] M. A. Reshchikov, Mater. Res. Soc. Symp. Proc. **1035**, 1035 (2007).

[30] P. E. Blöchl, Phys. Rev. B **50**, 17953 (1994).

[31] G. Kresse and D. Joubert, Phys. Rev. B **59**, 1758 (1999).

[32] A. V. Krukau, O. A. Vydrov, A. F. Izmaylov, and G. E. Scuseria, J. Chem. Phys. **125**, 224106 (2006).

[33] G. Kresse and J. Furthmüller, Phys. Rev. B **54**, 11169 (1996).

[34] S. Lany and A. Zunger, Phys. Rev. B **80**, 085202 (2009).

[35] G. Miceli, W. Chen, I. Reshetnyak, and A. Pasquarello, Phys. Rev. B **97**, 121112(R) (2018).

[36] D. O. Demchenko, I. C. Diallo, and M. A. Reshchikov, Phys. Rev. B **97**, 205205 (2018).

[37] P. Deák, M. Lorke, B. Aradi, and T. Frauenheim, Phys. Rev. B **99**, 085206 (2019).

[38] F. Oba, A. Togo, I. Tanaka, J. Paier, and G. Kresse, Phys. Rev. B **77**, 245202 (2008).

[39] D. C. Reynolds, D. C. Look, B. Jogai, C. W. Litton, G. Cantwell, and W. C. Harsch, Phys. Rev. B **60**, 2340 (1999).

[40] A. Baldereschi, Phys. Rev. B **7**, 5212 (1973).

[41] S. B. Zhang and J. E. Northrup, Phys. Rev. Lett. **67**, 2339 (1991).

[42] C. Freysoldt, B. Grabowski, T. Hickel, J. Neugebauer, G. Kresse, A. Janotti, and C. G. Van de Walle, Rev. Mod. Phys. **86**, 253 (2014).

[43] A. Janotti and C. G. Van de Walle, Phys. Rev. B **76**, 165202 (2007).

[44] Y. K. Frodason, K. M. Johansen, T. S. Bjørheim, B. G. Svensson, and A. Alkauskas, Phys. Rev. B **95**, 094105 (2017).

[45] J. L. Lyons, J. B. Varley, D. Steiauf, A. Janotti, and C. G. V. de Walle, J. Appl. Phys. **122**, 035704 (2017).

[46] Y. Kumagai and F. Oba, Phys. Rev. B **89**, 195205 (2014).

[47] C. Freysoldt, J. Neugebauer, and C. G. Van de Walle, Phys. Rev. Lett. **102**, 016402 (2009).

[48] A. Alkauskas, J. L. Lyons, D. Steiauf, and C. G. Van de Walle, Phys. Rev. Lett. **109**, 267401 (2012).

[49] A. Alkauskas, M. D. McCluskey, and C. G. Van de Walle, J. Appl. Phys. **119**, 181101 (2016).

[50] Y. K. Frodason, K. M. Johansen, T. S. Bjørheim, B. G. Svensson, and A. Alkauskas, Phys. Rev. B **97**, 104109 (2018).

[51] S. Kim, S. N. Hood, and A. Walsh, Wmdgroup/carriercapture.jl: Carriercapture.jl, 2019.

[52] C. G. Van de Walle, Phys. Rev. Lett. **85**, 1012 (2000).

[53] M. McCluskey and S. Jokela, Phys. B Condens. Matter **401**, 355 (2007).

[54] A. Janotti and C. G. V. de Walle, Rep. Prog. Phys. **72**, 126501 (2009).

[55] L. Vines and A. Kuznetsov, Semicond. Semimet. **88**, 67 (2013).

[56] Y. Y. Sun, T. A. Abtew, P. Zhang, and S. B. Zhang, Phys. Rev. B **90**, 165301 (2014).

[57] B. K. Meyer, A. Hofstaetter, and V. V. Laguta, Phys. B Condens. Matter **376–377**, 682 (2006).

[58] M.-H. Du and S. B. Zhang, Phys. Rev. B **80**, 115217 (2009).

[59] A. Alkauskas, Q. Yan, and C. G. Van de Walle, Phys. Rev. B **90**, 075202 (2014).

[60] C. G. Van de Walle and J. Neugebauer, J. Appl. Phys. **95**, 3851 (2004).

[61] E. V. Lavrov, F. Börrnert, and J. Weber, Phys. Rev. B **71**, 035205 (2005).

[62] K. M. Johansen, H. Haug, E. Lund, E. V. Monakhov, and B. G. Svensson, Appl. Phys. Lett. **97**, 211907 (2010).

[63] F. Herklotz, K. M. Johansen, A. Galeckas, T. N. Sky, and B. G. Svensson, Phys. Status Solidi B **253**, 273 (2015).

[64] D. Steiauf, J. L. Lyons, A. Janotti, and C. G. Van de Walle, APL Mater. **2**, 096101 (2014).

[65] K. M. Johansen, J. S. Christensen, E. V. Monakhov, A. Y. Kuznetsov, and B. G. Svensson, Appl. Phys. Lett. **93**, 152109 (2008).

[66] T. N. Sky, K. M. Johansen, Y. K. Frodason, B. G. Svensson, and L. Vines, J. Appl. Phys. **124**, 245702 (2018).

[67] C. E. Dreyer, A. Alkauskas, J. L. Lyons, A. Janotti, and C. G. Van de Walle, Annu. Rev. Mater. Sci. **48**, 1 (2018).

[68] V. A. Nikitenko, J. Appl. Spectrosc. **57**, 783 (1992).

[69] D. O. Demchenko, I. C. Diallo, and M. A. Reshchikov, Phys. Rev. Lett. **110**, 087404 (2013).

[70] S. G. Christenson, W. Xie, Y. Y. Sun, and S. B. Zhang, J. Appl. Phys. **118**, 135708 (2015).

[71] D. O. Demchenko, I. C. Diallo, and M. A. Reshchikov, J. Appl. Phys. **119**, 035702 (2016).

[72] M. A. Reshchikov, M. Vorobiov, D. O. Demchenko, U. Özgür, H. Morkoç, A. Lesnik, M. P. Hoffmann, F. Hörich, A. Dadgar, and A. Strittmatter, Phys. Rev. B **98**, 125207 (2018).

[73] M. A. Reshchikov, AIP Conf. Proc. **1583**, 127 (2014).

[74] M. A. Reshchikov, V. Avrutin, N. Izyumskaya, R. Shimada, H. Morkoç, and S. W. Novak, J. Vac. Sci. Technol. B **27**, 1749 (2009).

[75] M. A. Reshchikov, J. D. McNamara, A. Usikov, H. Helava, and Y. Makarov, Phys. Rev. B **93**, 081202(R) (2016).

[76] M. Reshchikov, Y. Moon, X. Gu, B. Nemeth, J. Nause, and H. Morkoç, Phys. B Condens. Matter **376–377**, 715 (2006).

[77] R. Heinhold, A. Neiman, J. V. Kennedy, A. Markwitz, R. J. Reeves, and M. W. Allen, Phys. Rev. B **95**, 054120 (2017).

[78] K. E. Knutsen, K. M. Johansen, P. T. Neuvonen, B. G. Svensson, and A. Y. Kuznetsov, J. Appl. Phys. **113**, 023702 (2013).

[79] P. T. Neuvonen, L. Vines, B. G. Svensson, and A. Y. Kuznetsov, Phys. Rev. Lett. **110**, 015501 (2013).

[80] A. Y. Azarov, K. E. Knutsen, P. T. Neuvonen, L. Vines, B. G. Svensson, and A. Y. Kuznetsov, Phys. Rev. Lett. **110**, 175503 (2013).

[81] R. Dingle, Phys. Rev. Lett. **23**, 579 (1969).

[82] D. Byrne, F. Herklotz, M. O. Henry, and E. McGlynn, J. Phys. Condens. Matter **24**, 215802 (2012).

[83] K. M. Johansen, A. Zubiaga, I. Makkonen, F. Tuomisto, P. T. Neuvonen, K. E. Knutsen, E. V. Monakhov, A. Y. Kuznetsov, and B. G. Svensson, Phys. Rev. B **83**, 245208 (2011).

[84] E. V. Lavrov, F. Herklotz, and J. Weber, Phys. Rev. B **79**, 165210 (2009).

[85] J. Cullen, D. Byrne, K. Johnston, E. McGlynn, and M. O. Henry, Appl. Phys. Lett. **102**, 192110 (2013).

[86] J. R. Haynes, Phys. Rev. Lett. **4**, 361 (1960).

[87] K. Tang, R. Gu, S. Zhu, Z. Xu, Y. Shen, J. Ye, and S. Gu, Opt. Mater. Express **7**, 1169 (2017).

[88] H. Atzmüller, F. Fröschl, and U. Schröder, Phys. Rev. B **19**, 3118 (1979).

[89] D. Pan, Solid State Commun. **37**, 375 (1981).

[90] B. K. Meyer, J. Sann, S. Lautenschläger, M. R. Wagner, and A. Hoffmann, Phys. Rev. B **76**, 184120 (2007).

[91] J. F. Janak, Phys. Rev. B **18**, 7165 (1978).

[92] W. Chen and A. Pasquarello, Phys. Rev. B **88**, 115104 (2013).

[93] I. Souza, J. Íñiguez, and D. Vanderbilt, Phys. Rev. Lett. **89**, 117602 (2002).